

Organ-aware Multi-scale Medical Image Segmentation Using Text Prompt Engineering

Wenjie Zhang¹, Ziyang Zhang², Mengnan He², and Jiancheng Ye^{1,2*}

¹ Weill Cornell Medicine, Cornell University, New York, USA

² Northwestern University, Evanston, USA

Abstract. Accurate segmentation is essential for effective treatment planning and disease monitoring. Existing medical image segmentation methods predominantly rely on uni-modal visual inputs, such as images or videos, requiring labor-intensive and precise manual annotations. Additionally, medical imaging techniques capture multiple intertwined organs within a single scan, further complicating segmentation accuracy. To address these challenges, MedSAM, a large-scale medical segmentation model based on the Segment Anything Model (SAM), was developed to enhance segmentation accuracy by integrating image features with user-provided prompts. While MedSAM has demonstrated strong performance across various medical segmentation tasks, it primarily relies on geometric prompts (e.g., points and bounding boxes) and lacks support for text-based prompts, which could help specify subtle or ambiguous anatomical structures. To overcome these limitations, we propose the Organ-aware Multi-scale Text-guided Medical Image Segmentation Model (OMT-SAM) for multi-organ segmentation. Our approach introduces CLIP encoders as a novel image-text prompt encoder, operating with the geometric prompt encoder to provide informative contextual guidance. We pair descriptive textual prompts with corresponding images, processing them through pre-trained CLIP encoders and a cross-attention mechanism to generate fused image-text embeddings. Additionally, we extract multi-scale visual features from MedSAM, capturing fine-grained anatomical details at different levels of granularity. We evaluate OMT-SAM on the FLARE 2021 Grand Challenge dataset, benchmarking its performance against existing segmentation methods and alternative prompting strategies. Empirical results demonstrate that OMT-SAM achieves a mean Dice Similarity Coefficient of 0.937, outperforming MedSAM (0.893) and other segmentation models, highlighting its superior capability in handling complex medical image segmentation tasks.

Keywords: Medical Image Segmentation · CLIP · MedSAM · Text Prompt.

1 Introduction

Accurate segmentation of abdominal organs is essential for radiotherapy treatment planning and disease monitoring. Traditional automatic segmentation methods often struggle with the complexity of organ shapes, their close proximity to

one another, and the high cost of manual annotation [16]. These challenges can lead to difficulties in segmenting intricate organs and tissues, ultimately reducing the robustness and reliability of segmentation results. To mitigate the burden of manual labeling and enhance segmentation efficiency, prompt-based interactive segmentation [21] has emerged as a promising approach. By providing hints such as points, bounding boxes, or text descriptions, users can guide models to segment target organs or tissues efficiently [10]. This approach not only accelerates the segmentation process but also leverages expert knowledge to enhance accuracy in complex tasks. However, using pinpoints and bounding boxes in medical settings often requires specialized clinical knowledge, such as identifying diseased areas like nodules. Generating such domain-specific annotations typically needs input from well-trained clinicians and medical professionals, making the process resource-intensive. Additionally, while text prompts may seem intuitive, finding the right model to effectively map medical terminology to image features presents its own set of challenges. These factors contribute to the technical difficulty of developing an effective deep learning model for medical image segmentation. These factors contribute to the technical difficulty of developing an effective deep learning model for medical image segmentation.

To address these aforementioned challenges, we propose the Organ-aware Multi-scale Text-guided Medical Image Segmentation Model (OMT-SAM), with a novel design of image-text prompt encoder and further integration of multi-scale feature representations. The pre-trained CLIP encoders [1] were used to generate paired image and text representations, which are then processed through a cross-attention layer to produce fused image-text prompt embeddings. The proposed method is capable of guiding MedSAM [13] to segment fine-grained organ details and providing flexibility in segmenting specific organs within complex medical images containing multiple targets. Empirical results demonstrate that OMT-SAM surpasses the original MedSAM across various prompting strategies and outperforms other deep learning-based segmentation models. In summary, our contributions are as follows: (1) We introduce a fused image-text prompt encoder that enhances SAM’s ability to segment abdominal organs in CT scans with improved contextual understanding. (2) By merging visual features at multiple granularities, our model achieves finer organ detail recognition, leading to more precise segmentation masks. (3) Our method outperforms existing segmentation models, establishing a new benchmark for abdominal organ segmentation in medical imaging. The link of anonymous codebase is <https://anonymous.4open.science/r/OMT-SAM-D6A2/README.md>.

2 Related Works

Abdominal organs play a crucial role in various clinical applications like surgical navigation. However, manual annotation of CT, MRI, or ultrasound images is time-consuming and susceptible to inter-observer variability, making segmentation a challenging task [16] [8] [9]. Classical methods such as thresholding, region growing, and edge detection are limited by anatomical variations [7]. While deep

learning techniques, especially U-Net [20] and its derivatives like PSPNet [22] and TransUNet [2], have significantly improved segmentation accuracy by leveraging spatial information and long-range dependencies. For example, U-Net and TransUNet have been shown to achieve a mean accuracy of 0.839 and 0.872 [11] in the Flare 2021 grand challenge dataset [14]. Segment Anything (SAM) [10] has sparked interest in adapting foundation models to medical image segmentation, resulting in the development of specialized versions like MedSAM [13]. MedSAM refines SAM’s approach for medical imaging, enhancing segmentation accuracy and enabling applications in automated disease diagnosis and surgical planning. Prompt-based segmentation, where users provide guidance (e.g., points, bounding boxes, and text descriptions) [15], further improves segmentation accuracy and efficiency [17]. In this work, we proposed and validated that the integration of models like Contrastive Language-Image Pre-training (CLIP) [18] and MedSAM [13], which combine image and text prompts, has the capability to lead to more precise segmentation by interpreting medical terminology and capturing subtle anatomical features.

3 Methodology

An overview of the proposed framework is illustrated in Figure 1, which can be mainly divided into four parts that are introduced hereafter.

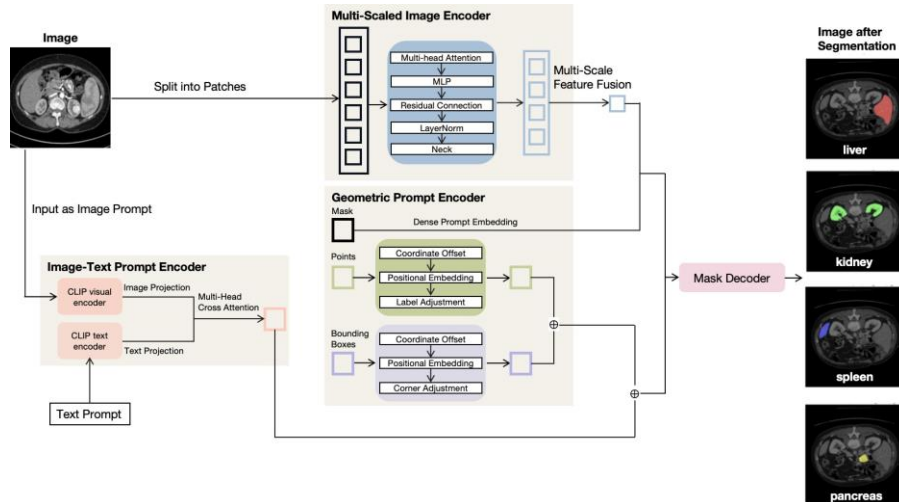


Fig. 1. The overview of our proposed OMT-SAM framework, which consists of four main components: a multi-scaled image encoder, a geometric prompt encoder, an image-text prompt encoder and a mask decoder

3.1 Multi-scaled Image Encoder

Our multi-scaled image encoder is built upon the Vision Transformer (ViT) [4], which excels at extracting image features. The first step is to produce patch embeddings, which divide the input images into fixed-size patches. These patches are then projected into a high-dimensional feature space through a convolutional operation. Then transformer blocks process these patch embeddings by a self-attention mechanism. To fully leverage deeper representations, we select the last four-layer visual features from the different transformer layers. These outputs are passed through a neck module consisting of sequential 1×1 and 3×3 convolutions. This module is designed to enhance feature extraction by providing multi-scale features, which are crucial for capturing fine-grained details of organs and their boundaries.

3.2 Geometric Prompt Encoder

The geometric prompt encoder plays a critical role in enabling the model to understand and incorporate input prompts, such as points and bounding boxes. MedSAM employs distinct embedding methods for point and bounding box inputs. Depending on the point labels - such as positive, negative, and invalid points - it utilizes different embedding strategies. The feature representations for the bounding box inputs are generated by mapping the coordinates of the two corners to a fixed embedding space. For each point or bounding box, the geometric prompt encoder applies positional encoding techniques to ensure that the prompt information is fully integrated with the spatial and geometric features of the image. When handling masks, the encoder uses a convolutional network for downsampling, progressively mapping the input masks to a higher-dimensional feature space while incorporating the geometric information of the image. The dimensionality and spatial resolution of these embeddings are dynamically adjusted based on the image size and embedding dimension, ensuring that the mask information is effectively included in subsequent model processing along with other geometric prompts. If no point or bounding box input is provided, the encoder processes the input using a "silent" embedding to ensure that the model can still generate meaningful representations, even in the absence of these prompts. As the BCE Loss alone cannot capture the subtle details in scenarios where the target is small compared to the background, we incorporate the Dice Loss to more effectively optimize the segmentation of small targets [19]. We optimize the model using backpropagation and gradient descent, with a combined loss of Dice Loss and BCE Loss, formulated as follows,

$$L_{\text{total}} = \lambda_1 L_{\text{Dice}} + \lambda_2 L_{\text{BCE}} \quad (1)$$

where λ_1 and λ_2 are the weighting factors that balance the contribution of each loss term. The learned geometric embeddings were fed into the mask decoder.

3.3 Image-text Prompt Encoder

For textual prompts, we utilize the pre-trained CLIP model, which consists of two components: a visual encoder and a text encoder. The CLIP model is pre-trained on a large-scale dataset of image-text pairs, which helps the model capture generalizable knowledge for a variety of image-text tasks. It maps both images and text to a shared feature space, enabling the model to understand and process natural language instructions in the context of medical image segmentation tasks. This cross-modal alignment allows CLIP to effectively interpret textual prompts such as "segment the liver" and associate them with corresponding image features. The input image to be segmented is resized to 224×224 pixels, and a paired textual description is provided to the CLIP model. The visual encoder processes the image, generating a dense image embedding that represents the image's visual features. Meanwhile, the text encoder processes the textual description and generates a textual embedding that captures the semantic meaning of the input prompt. These embeddings are then aligned through a cross-attention mechanism, which ensures that the model can fuse the image and text features, allowing for a more nuanced understanding of the prompt. This fusion enables the model to effectively combine both the visual context and textual instruction for accurate segmentation.

3.4 Mask Decoder

The mask decoder is responsible for generating the final segmentation mask by fusing multi-scale and multi-modal information. This module is key to aligning features from different scales, ensuring that both fine-grained and global features contribute to the final segmentation. A low-resolution candidate mask is first generated through mask upsampling, which reduces computational overhead and provides a coarse segmentation. This candidate mask is then upsampled to match the original image resolution, yielding the final, high-resolution segmentation mask.

4 Experiments and Results

4.1 Dataset and Evaluation Metrics

We used the Flare 2021 grand challenge dataset [14], which includes 361 labeled 3D medical images for liver, kidney, spleen, and pancreas segmentation. Due to the high computational demands of volumetric data, we pre-processed the images by extracting 2D slices and saving them as compressed .npz files. The data set was organized into folders for each organ, with the corresponding ground truth and textual descriptions for each segmentation task. The Dice Similarity Coefficient (DSC) [23], Normalized Surface Distance (NSD) [5], and Hausdorff Distance at 95th Percentile (HD95) [6] are used to evaluate the segmentation performance of the abdominal organs.

4.2 Implementation Details

The proposed framework is implemented on the PyTorch library with one NVIDIA 80G H100 GPU. We adopted the original MedSAM as the base and loaded its official weights. During the training and test step, the model is trained for 30 epochs on the Flare dataset with a batch size of 8, using the Adam optimizer (learning rate is 0.0001). The baseline models are also trained for 30 epochs on the Flare dataset with the same hyperparameters.

4.3 Comparison with State-of-the-art

Quantitative comparisons We compared the proposed model with advanced baselines, including MedSAM, U-Net (2D and 3D) [20], TransUNet (2D and 3D) [2], PSPNet [22], FPN [12], and DeepLabV3+ [3]. Table 1 shows the average Dice similarity coefficient (DSC) for the models on the FLARE 2021 dataset. Our model achieved an average DSC of 0.937, outperforming original MedSAM, which achieved a DSC of 0.893. The performance of the other baseline models (e.g. U-Net (2D), TransUNet (2D), PSPNet, FPN, DeepLabV3+) was relatively poor in segmentation, particularly for organs with complex structures and blurry boundaries, such as the spleen and pancreas. For these organs, the DSC and NSD for the pancreas were found to be less than 0.1, and thus we excluded these values from the mean calculation. In conclusion, our OMT-SAM demonstrated superior performance in all the other baselines, particularly in handling complex organ boundaries and overlapping regions.

Table 1. Comparison of Segmentation Models.

| Method | Mean DSC | Mean NSD |
|---------------|----------|----------|
| OMT-SAM | 0.937 | 0.969 |
| MedSAM | 0.893 | 0.927 |
| U-Net(2D) | 0.516 | 0.534 |
| U-Net(3D) | 0.839 | 0.621 |
| TransUNet(2D) | 0.463 | 0.478 |
| TransUNet(3D) | 0.872 | 0.699 |
| PSPNet | 0.480 | 0.502 |
| FPN | 0.502 | 0.525 |
| DeepLabV3+ | 0.503 | 0.523 |

The Dice scores in Table 2 compare the performance of different models on various abdominal organs. As shown, our model outperforms MedSAM, U-Net, TransUNet, PSPNet, FPN, and DeepLabV3+ across all organs, particularly on challenging organs such as the spleen and pancreas. The results highlight the superior ability of OMT-SAM in accurately segmenting organs with complex boundaries, making it an ideal choice for abdominal organ segmentation tasks.

Table 2. Dice scores for different models on various abdominal organs. Note: "-" indicates values less than 0.1 for the Pancreas column.

| Method | Liver | Kidney | Spleen | Pancreas |
|---------------|---------------|----------------|---------------|---------------|
| OMT-SAM | 0.972 ± 0.003 | 0.956 ± 0.006 | 0.971 ± 0.006 | 0.848 ± 0.015 |
| MedSAM | 0.925 ± 0.013 | 0.921 ± 0.0167 | 0.943 ± 0.012 | 0.783 ± 0.020 |
| U-Net(2D) | 0.765 ± 0.053 | 0.532 ± 0.055 | 0.251 ± 0.008 | - |
| U-Net(3D) | 0.942 ± 0.025 | 0.815 ± 0.151 | 0.933 ± 0.045 | 0.666 ± 0.101 |
| TransUNet(2D) | 0.623 ± 0.008 | 0.529 ± 0.018 | 0.236 ± 0.021 | - |
| TransUNet(3D) | 0.947 ± 0.029 | 0.922 ± 0.0121 | 0.923 ± 0.038 | 0.695 ± 0.093 |
| PSPNet | 0.752 ± 0.045 | 0.450 ± 0.044 | 0.237 ± 0.010 | - |
| FPN | 0.772 ± 0.050 | 0.494 ± 0.045 | 0.240 ± 0.007 | - |
| DeepLabV3+ | 0.780 ± 0.048 | 0.518 ± 0.051 | 0.212 ± 0.016 | - |

Qualitative comparison Figure 2 presents a visual comparison of segmentation results, where we observe that OMT-SAM outperforms MedSAM, particularly in detailing complex organ boundaries. OMT-SAM shows a superior ability to delineate organs such as kidney and pancreas, where it captures intricate boundaries and small anatomical structures with greater precision. By using text prompts such as "segment the liver," OMT-SAM effectively leverages cross-modal attention to fuse image and text features, leading to improved segmentation accuracy.

4.4 Ablation studies

We conducted ablation studies to assess the impact of different components in our model. The results of these experiments are summarized in Table 3.

Table 3. Ablation Study Results

| Experiment | Mean DSC | Mean NSD | Mean HD95 |
|------------------------------------|----------|----------|-----------|
| Full OMT-SAM Model | 0.937 | 0.969 | 17.385 |
| OMT-SAM without Multi-Feature | 0.936 | 0.967 | 14.938 |
| OMT-SAM without Image-text Encoder | 0.934 | 0.965 | 19.430 |

The results clearly show that the novel image-text prompt encoder and multi-scale feature extraction improve the segmentation performance significantly. Specifically, when the multi-feature part is removed, the mean DSC decreases by 0.001, and the mean NSD drops by 0.002. However, the most notable change is in the mean HD95, which decreases by more than 2. This reduction in HD suggests that the quality of the boundary delineation improves. Removing the image-text encoder results in a drop in all these of three metrics, which means the model loses some of its ability to align the image and text features effectively, leading to less accurate segmentation predictions. The ablation study demonstrates that both the image-text encoder and multi-feature extraction significantly contribute to the enhanced segmentation performance of OMT-SAM.

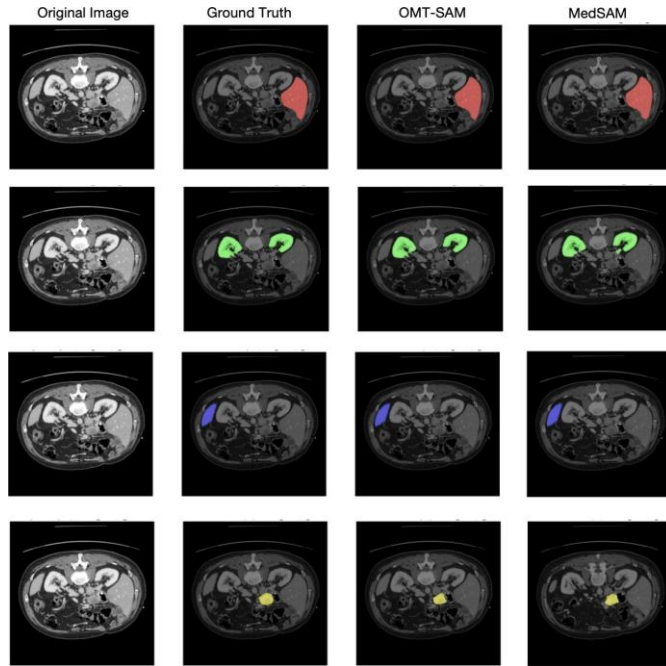


Fig. 2. Visual Comparison of Segmentation Results. From top to bottom, the organs are liver, kidney, spleen, and pancreas.

5 Conclusion

Compared to traditional methods that heavily depend on manual annotations, our multimodal framework offers several advantages. First, CLIP’s ability to map medical texts enables it to interpret a wide range of clinical terms and simple instructions, effectively linking them to anatomical structures. Second, the integration of multimodal prompts allows the model to accurately differentiate and segment multiple organs or lesions, even within complex abdominal anatomies. Lastly, the interactive prompting method provides clinicians with a fast and intuitive way to refine and customize segmentation results, ensuring robust performance across anatomical variations and diverse lesion patterns.

Experimental results demonstrate that OMT-SAM significantly reduces the reliance on manual labeling while delivering state-of-the-art and comparable performance in abdominal organ segmentation tasks. The quantitative and qualitative results demonstrate that our model outperforms MedSAM and other baseline methods in abdominal organ segmentation tasks, especially in segmentation accuracy, boundary matching, and surface consistency. This advancement lays a strong foundation for large-scale clinical applications, paving the way for more efficient and precise medical imaging workflows.

References

1. Boecking, B., Usuyama, N., Bannur, S., Castro, D.C., Schwaighofer, A., Hyland, S., Wetscherek, M., Naumann, T., Nori, A., Alvarez-Valle, J., Poon, H., Oktay, O.: Making the Most of Text Semantics to Improve Biomedical Vision–Language Processing, p. 1–21. Springer Nature Switzerland (2022). https://doi.org/10.1007/978-3-031-20059-5_1, http://dx.doi.org/10.1007/978-3-031-20059-5_1
2. Chen, J., Lu, Y., Yu, Q., Luo, X., Adeli, E., Wang, Y., Lu, L., Yuille, A.L., Zhou, Y.: Transunet: Transformers make strong encoders for medical image segmentation (2021), <https://arxiv.org/abs/2102.04306>
3. Chen, L.C., Zhu, Y., Papandreou, G., Schroff, F., Adam, H.: Encoder-decoder with atrous separable convolution for semantic image segmentation (2018), <https://arxiv.org/abs/1802.02611>
4. Dosovitskiy, A., Beyer, L., Kolesnikov, A., Weissenborn, D., Zhai, X., Unterthiner, T., Dehghani, M., Minderer, M., Heigold, G., Gelly, S., Uszkoreit, J., Houslyby, N.: An image is worth 16x16 words: Transformers for image recognition at scale (2021), <https://arxiv.org/abs/2010.11929>
5. Fischl, B., Salat, D.H., Busa, E., Albert, M., Dieterich, M., Haselgrove, C., Van Der Kouwe, A., Killiany, R., Kennedy, D., Klaveness, S., et al.: Whole brain segmentation: automated labeling of neuroanatomical structures in the human brain. *Neuron* **33**(3), 341–355 (2002)
6. Huttenlocher, D., Klanderman, G., Rucklidge, W.: Comparing images using the hausdorff distance. *IEEE Transactions on Pattern Analysis and Machine Intelligence* **15**(9), 850–863 (1993). <https://doi.org/10.1109/34.232073>
7. Jähne, B.: Digital image processing. Springer Science & Business Media (2005)
8. Joskowicz, L., Cohen, D., Caplan, N., Sosna, J.: Inter-observer variability of manual contour delineation of structures in ct. *European radiology* **29**, 1391–1399 (2019)
9. Kavur, A.E., Gezer, N.S., Barış, M., Aslan, S., Conze, P.H., Groza, V., Pham, D.D., Chatterjee, S., Ernst, P., Özkan, S., et al.: Chaos challenge-combined (ctmr) healthy abdominal organ segmentation. *Medical image analysis* **69**, 101950 (2021)
10. Kirillov, A., Mintun, E., Ravi, N., Mao, H., Rolland, C., Gustafson, L., Xiao, T., Whitehead, S., Berg, A.C., Lo, W.Y., et al.: Segment anything. In: Proceedings of the IEEE/CVF International Conference on Computer Vision. pp. 4015–4026 (2023)
11. Liao, M., Tang, H., Li, X., Vijayakumar, P., Arya, V., Gupta, B.B.: A lightweight network for abdominal multi-organ segmentation based on multi-scale context fusion and dual self-attention. *Information Fusion* **108**, 102401 (2024)
12. Lin, T.Y., Dollár, P., Girshick, R., He, K., Hariharan, B., Belongie, S.: Feature pyramid networks for object detection (2017), <https://arxiv.org/abs/1612.03144>
13. Ma, J., He, Y., Li, F., Han, L., You, C., Wang, B.: Segment anything in medical images. *Nature Communications* **15**(1), 654 (2024)
14. Ma, J., Zhang, Y., Gu, S., An, X., Wang, Z., Ge, C., Wang, C., Zhang, F., Wang, Y., Xu, Y., Gou, S., Thaler, F., Payer, C., Štern, D., Henderson, E.G., McSweeney, D.M., Green, A., Jackson, P., McIntosh, L., Nguyen, Q.C., Qayyum, A., Conze, P.H., Huang, Z., Zhou, Z., Fan, D.P., Xiong, H., Dong, G., Zhu, Q., He, J., Yang, X.: Fast and low-gpu-memory abdomen ct organ segmentation: The flare challenge. *Medical Image Analysis* **82**, 102616 (2022)
15. Mashburn, D.N., Lynch, H.E., Ma, X., Hutson, M.S.: Enabling user-guided segmentation and tracking of surface-labeled cells in time-lapse image sets of living tissues. *Cytometry Part A* **81**(5), 409–418 (2012)

16. Masood, S., Sharif, M., Masood, A., Mussarat, Y., Raza, M.: A survey on medical image segmentation. *Current Medical Imaging Reviews* **11**, 3–14 (02 2015). <https://doi.org/10.2174/157340561101150423103441>
17. Olabarriaga, S.D., Smeulders, A.W.: Interaction in the segmentation of medical images: A survey. *Medical image analysis* **5**(2), 127–142 (2001)
18. Radford, A., Kim, J.W., Hallacy, C., Ramesh, A., Goh, G., Agarwal, S., Sastry, G., Askell, A., Mishkin, P., Clark, J., et al.: Learning transferable visual models from natural language supervision. In: *International conference on machine learning*. pp. 8748–8763. PMLR (2021)
19. Rajput, V.: Robustness of different loss functions and their impact on networks learning capability (2021), <https://arxiv.org/abs/2110.08322>
20. Ronneberger, O., Fischer, P., Brox, T.: U-net: Convolutional networks for biomedical image segmentation. In: *Medical image computing and computer-assisted intervention—MICCAI 2015: 18th international conference, Munich, Germany, October 5–9, 2015, proceedings, part III* **18**. pp. 234–241. Springer (2015)
21. Wang, G., Li, W., Zuluaga, M.A., Pratt, R., Patel, P.A., Aertsen, M., Doel, T., David, A.L., Deprest, J., Ourselin, S., Vercauteren, T.: Interactive medical image segmentation using deep learning with image-specific fine tuning. *IEEE Transactions on Medical Imaging* **37**(7), 1562–1573 (2018). <https://doi.org/10.1109/TMI.2018.2791721>
22. Zhao, H., Shi, J., Qi, X., Wang, X., Jia, J.: Pyramid scene parsing network. In: *2017 IEEE Conference on Computer Vision and Pattern Recognition (CVPR)*. pp. 6230–6239 (2017). <https://doi.org/10.1109/CVPR.2017.660>
23. Zhao, R., Qian, B., Zhang, X., Li, Y., Wei, R., Liu, Y., Pan, Y.: Rethinking dice loss for medical image segmentation. In: *2020 IEEE International Conference on Data Mining (ICDM)*. pp. 851–860 (2020). <https://doi.org/10.1109/ICDM50108.2020.00094>